

A redshift – observation-time relation for gamma-ray bursts: evidence of a distinct sub-luminous population

E. J. Howell^{1*} and D. M. Coward¹

¹*School of Physics, University of Western Australia, Crawley WA 6009, Australia*

5 June 2018

ABSTRACT

We show how the redshift and peak-flux distributions of gamma-ray bursts (GRBs) have an observation-time dependence that can be used to discriminate between different burst populations. We demonstrate how observation-time relations can be derived from the standard integral distributions and that they can differentiate between GRB populations detected by both the BATSE and *Swift* satellites. Using *Swift* data we show that a redshift–observation-time relation ($\log Z - \log T$) is consistent with both a peak-flux–observation-time relation ($\log P - \log T$) and a standard $\log N - \log P$ brightness distribution. As the method depends only on rarer small- z events, it is invariant to high- z selection effects. We use the $\log Z - \log T$ relation to show that sub-luminous GRBs are a distinct population occurring at a higher rate of order $150_{-90}^{+180} \text{Gpc}^{-3} \text{yr}^{-1}$. Our analysis suggests that GRB 060505 – a relatively nearby GRB observed without any associated supernova – is consistent with a sub-luminous population of bursts. Finally, we show that our relations can be used as a consistency test for some of the proposed GRB spectral energy correlations.

Key words: gamma-rays: bursts – gamma-ray: observations – methods:data analysis – supernovae: general – cosmology: miscellaneous

1 INTRODUCTION

Multi-wavelength observations have shown that γ -ray bursts (GRBs) are the most luminous¹ and distant transient events in the Universe (Greiner et al. 2008; Cucchiara et al. 2011). GRBs have been generally categorized into two populations: spectrally soft long duration bursts related to core-collapse events (LGRBs/Type II); harder short duration bursts possibly resulting from compact star mergers (SGRB/Type I).

In addition to these two main populations of bursts it has been suggested there exist two sub-populations: sub-luminous GRBs (SL-GRBs) and SGRBs with extended emissions (SGRB-EE). SL-GRBs are of the long-duration type and have isotropic equivalent γ -ray luminosities 2-3 orders of magnitude below classical LGRBs (Coward 2005; Murase et al. 2006; Guetta & Della Valle 2007; Imerito et al. 2008). The lower energy emissions mean they are only detected at low- z – as such, four of the six GRBs with unambiguous spectroscopically confirmed GRB-supernova associations were from this category. SGRB-EEs emissions have been given a separate classification in the second *Swift* catalogue (Sakamoto et al. 2011). These bursts

show an initial SGRB like short hard spike (< 2 s) followed by a faint softer emission ($\gtrsim 100$ s) (Norris & Bonnell 2006; Norris et al. 2011; Page et al. 2006; Perley et al. 2008; Zhang 2011).

There is still no clear consensus that these sub-categories arise from different progenitor systems or are simply rarer events from the tail of the respective short/long burst distributions. Attempts to address this have generally been based on statistical arguments (Soderberg et al. 2006; Guetta & Della Valle 2007), fits to the $\log N - \log P$, peak flux, or ‘brightness distribution’ of bursts (Pian et al. 2006) or through simulation (Coward 2005; Virgili et al. 2008).

The goal of this paper is to demonstrate an alternative strategy using the relative time records of the bursts. This approach exploits the fact that different astrophysical transient populations will have different local rate densities. We show that by recording the arrival times of the rarest events in a time series e.g. the closest or brightest of a cosmological population, one can produce a rate dependent data set with a unique statistical signature (Coward & Burman 2005). By constraining the data using an observation-time dependent model that is highly sensitive to the rate density, we demonstrate how this alternative approach can untangle different source populations. In this study we will specifically address

* E-mail:eric.howell@uwa.edu.au

¹ In terms of electromagnetic radiation per unit solid angle.

the issue of whether SL-GRBs are a distinct population of GRBs. The outline of the paper is as follows:

In section 2 we present an overview of GRB population studies. Section 3 will set the scene in regards to the observation-time dependence of transient events and Section 4 will describe the data extraction methodologies used in this study. A standard theoretical framework will follow in Section 5.

Section 6 describes observation-time dependent models for both peak flux ($\log P - \log T$) and redshift ($\log Z - \log T$) showing how they follow seamlessly from the relative integral distributions of transient sources. In Section 7, parameters for both the BATSE² and *Swift* LGRB populations will be obtained using a standard differential $\log N - \log P$ distribution. These parameters will be used in Section 8 to constrain the peak-flux – observation-time data from both detectors using a $\log N - \log P$ model. Doing so demonstrates that the method is both consistent with a standard brightness distribution and is detector independent.

Section 9 will demonstrate the use of the previously derived parameters in the redshift – observation-time domain to constrain *Swift* data using the $\log Z - \log T$ model. In Section 10 we apply our methods to the *Swift* SL-GRB population to further demonstrate how the method can be used as a tool to discriminate between different source populations. We show that the method uses only the closest or brightest of a population; thus many of the selection biases that plague GRB observations can be bypassed. We discuss our findings and present our conclusions in Section 11.

2 GAMMA-RAY BURST POPULATIONS

The categorisation of GRBs was traditionally based on the bimodal distribution of T_{90} durations observed by BATSE³ (Kouveliotou et al. 1993) and their hardness ratio in the spectral domain. These criteria separated GRBs into hard SGRBs ($T_{90} < 2$ s; hard spectra) and softer LGRBs ($T_{90} \geq 2$ s; soft spectra).

Electromagnetic observations of LGRBs and SGRBs have provided strong evidence for different progenitors. LGRBs have been associated with the deaths of massive stars (Woosley & Bloom 2006; Hjorth 2003; Stanek 2003) and have subsequently been found in or near dense regions of active star-formation, predominantly dwarf starburst field galaxies (Fruchter et al. 2006). For SGRBs, which have contributed around 25% and 10% of the BATSE and *Swift* GRB samples respectively (Guetta & Stella 2009), the leading progenitor model is the merger of compact neutron stars and/or black hole binaries. The association of an older stellar population with these bursts is supported by their occurrence in both early and late-type galaxies, as well as field and cluster galaxies.

There exist, however, a number of ambiguities in the categorisation schemes of GRB populations. LGRBs, such

as GRB 060614 and GRB 060505, showed no evidence of a supernova, despite extensive follow up campaigns (Zhang 2006). Additionally, it has been suggested that the two closest recorded bursts, GRB 980425 (36 Mpc) and GRB 060218 (145 Mpc), along with GRB 031203, associated with a host galaxy at ~ 480 Mpc (Feng & Fox 2010) and GRB 100316D (Starling et al. 2011) ($z \sim 0.06$) make up a sub-class of SL-GRBs (Cobb et al. 2006; Liang et al. 2007; Guetta & Della Valle 2007; Virgili et al. 2009). This class of GRB have isotropic equivalent γ -ray energy emissions typically several orders of magnitude below those of standard long-duration GRBs (Murase et al. 2006; Guetta & Della Valle 2007; Imerito et al. 2008) suggesting that they could form a unique population of bursts that due to their relatively close proximity, must be occurring at a higher rate. The suggestion that SL-GRBs could be just normal LGRBs viewed off-axes has also been considered. This scenario was discounted by Daigne & Mochkovitch (2007) on statistical arguments as it would: a) result in a far higher local rate density than expected from LGRBs; b) require much narrower opening angles for LGRBs than typically derived from the breaks in afterglow lightcurves.

While the LGRB/supernovae connection is firm for the majority of these bursts, the progenitors behind SGRBs, which are rarer and more difficult to localise, are less certain (Mészáros 2006; Nakar 2007). Around 20% of the SGRBs detected by *Swift* have been followed by an extended emission lasting up to 100 s (Norris & Bonnell 2006; Perley et al. 2008) leading to suggestions that different progenitors produce these bursts (Norris et al. 2011). Candidate systems include the birth of a rapidly rotating protomagnetar produced through NS-NS merger or the accretion induced collapse of a white-dwarf (Metzger et al. 2008; Bucciantini et al. 2012). Chapman et al. (2009) further postulated that an initial spike produced by a soft γ -ray repeater (SGR) in a galaxy of close proximity could mimic a SGRB and found that a dual population luminosity function based on both SGR giant flare properties and SGRB luminosities was consistent with BATSE data. Interestingly, Vavrek et al. (2008) found the sky distribution of SGRBs to be anisotropic, implying a fraction at close proximity. Certainly, this suggests that classification of shorter duration bursts could be detector dependent (Page et al. 2006).

The various ambiguities have motivated a number of authors to re-define different classes of GRB through a number of properties including: spectral features, associated supernova, stellar population, host galaxy, location in the host galaxy and progenitor (Zhang et al. 2007; Bloom et al. 2008). This has led to the Type I (compact object mergers) and Type II (core-collapse) scheme.

The existence of a third population of bursts with intermediate duration has also been suggested. The first evidence of this additional population was provided through statistical analysis of the BATSE distribution (Mukherjee et al. 1998; Horváth 1998). This was later supported by analysis using data from the *BeppoSAX* (Horváth 2009), *RHESSI* (Řípa et al. 2009) and *Swift* satellites (Horváth et al. 2010a). To formulate a physical model for an intermediate class of bursts, Veres et al. (2010) showed that intermediate bursts have a lower than average peak flux distribution and suggested that this group, which are spectrally softer than LGRBs, may be related to X-ray flashes (XRFs) - these

² The Burst and Transient Source Experiment (BATSE) on the Compton Gamma-Ray Observatory was launched in 1991, and recorded over 2000 GRBs at a rate of around one a day for around 9 years of operation.

³ The T_{90} duration is the time during which the cumulative counts increase from 5% to 95% above background.

events have a dominant fraction of the total prompt fluence detected in X-ray rather than γ -ray.

3 EXPLOITING THE TIME DIMENSION

In this study we show that the time-record of GRB observations can be used as a tool to untangle different GRB populations. This largely overlooked quantity features strongly when one considers the observation of the *rarest* events in a population i.e. those events from the tail of the distribution which occur at low- z or have exceptional brightness in comparison with the average. Coward & Burman (2005) showed that these events possess a unique rate dependent statistical signature that can be described by the ‘probabilistic event horizon’ (PEH) concept. By recording successively rarer events as a function of observation-time, a data set can be produced and constrained by a rate dependent model (Coward et al. 2005; Howell et al. 2007a).

The basic concept is illustrated in Figure 1 showing the *Swift* LGRB peak flux data plotted against observation-time – we will often refer to such a time-series as $P(T)$ data (or $Z(T)$ in the redshift domain). Using a log-log plot it is apparent that successively brighter events have an observation-time dependence – the longer you observe, the greater the probability of observing an exceptionally bright event. Successively brighter events are indicated by squares – these are termed *PEH data*.

To constrain PEH data Howell et al. (2007b) extended the standard Euclidean derivation of a $\log N - \log P$ brightness distribution to show how including a time dependence could produce a peak flux–observation-time power law relation, $\log P - \log T$. They also illustrated how some processing could improve the amount of PEH data. In an application to *Swift* LGRB data, they demonstrated that the relation could be used as a probe of the event rate density of the sources. Additionally, the time dependence allowed the method to be used as a tool to predict the likelihood of future events.

In this paper we extend the previous study to present a

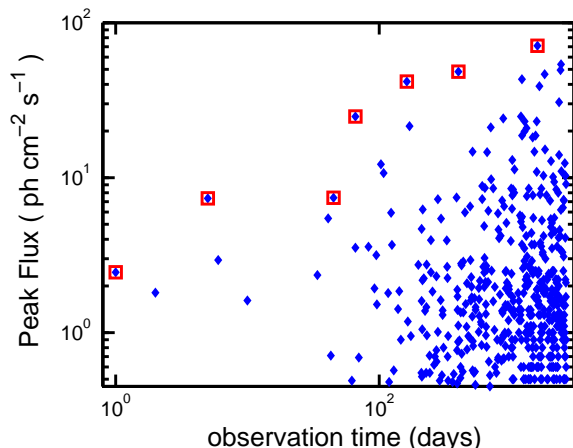


Figure 1. The *Swift* LGRB peak flux data plotted against observation-time. The plot illustrates how the probability of observing a bright event increases with observation-time. Successively brighter events - termed *PEH data* - are indicated by squares.

cosmological $\log P - \log T$ relation and show that the principle also extends to the redshift domain resulting in a $\log Z - \log T$ relation. For the latter case, the PEH data is a measure of the geometrical distribution of the source population. A $\log Z - \log T$ curve can be thought of as a horizon, defined by successively closer events, that approach a central observer as a function of observation-time (Coward & Burman 2005). As the successively closer events approach the local low- z regime rapidly, the GRB selection function (Coward 2007) and high- z selection effects such as the ‘redshift desert’ (Coward et al. 2008) have a negligible effect.

In the next section we will describe the data extraction principles that will be employed in the latter part of this study.

4 DATA EXTRACTION METHODOLOGY

To extract PEH data, we follow the *FromMax* method used by Howell et al. (2007b) to constrain the *Swift* LGRB sample. This invoked the temporal cosmological principle: for time scales that are short compared to the age of the Universe, there is nothing special about the time we switch on our detector. Therefore, the $P(T)$ time-series can be treated as closed loop, i.e. the start and endpoints of the time series can be joined and the start time set immediately after the brightest event. Successively brighter events and their observation-times are then recorded to produce a PEH data set of peak fluxes.

Figure 2 illustrates the concept. Using this procedure Howell et al. (2007b) showed that PEH data set can be obtained through both temporal directions – for simplicity we will only record data in the forward direction.

Employing this technique circumvents the possibility of a loud event occurring early in a time series; this would minimize the amount of output data as the next largest event would most probably occur near the end of the time series. Such a situation could be encountered by a detector operating with a high energy cutoff – a bias could be introduced producing a large number of events reaching the threshold. The advantage will become apparent in section 8.1 through analysis of the BATSE sample of bursts which contained a number of bright events at early observation-times.

Another feature of the *FromMax* method is that it ensures the total time duration of the PEH output is always equivalent to that of the total observation-time – this ensures a well ordered data sample is produced with a consistent time signature. We will show later through 2D Kolmogorov Smirnov testing that the improved data set retains the statistical signature of the original.

To apply the procedure to a sample of $P(T)$ data we first define the brightest event by P_* with an observation-time stamp T_* and denote the time of the last, most recent occurring event, as T_{\max} . Treating the data as a closed loop we reorder the data starting from the first event after P_* . The time stamps of the re-ordered data set $P^i(T_P^i)$ are now defined as:

$$T_P^i = \begin{cases} T - T_* & T > T_* \\ T + T_{\max} - T_* & T \leq T_* \end{cases} \quad (1)$$

To obtain a PEH data set we start to extract our data from the first minimum $P_{\min}^i = P_i^i < P_{i+1}^i$ – this additional

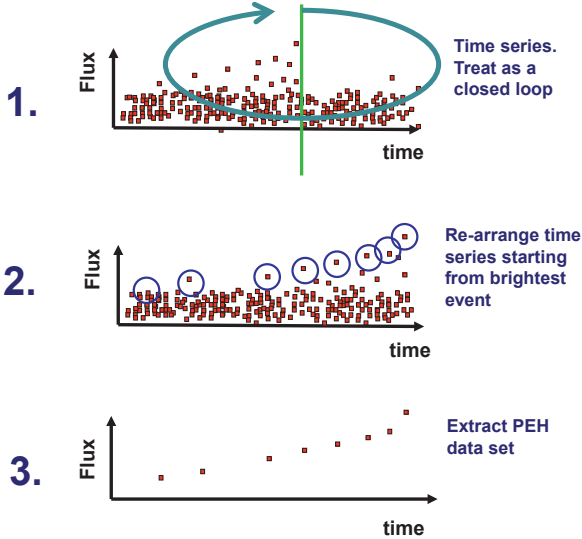


Figure 2. A cartoon illustrating the FromMAX data extraction principles of Howell et al. (2007b). Treating the data as a closed loop one can select a start point from which a data set of successively brighter events can be extracted. This data set is called PEH data.

step is to minimise the effect of an early bright event. A PEH data set is then obtained by recording successively brighter events $(P_i^1, T_{P,i}^1)$ satisfying the condition $P_{i+1}^1 > P_i^1$ for $P_i^1 \geq P_{\min}^1$.

To determine the PEH data set in the redshift domain one applies similar principles, treating the data as a closed loop but re-ordering the data from the first event after the closest redshift event Z_0 . The timestamps for the re-ordered set $Z^1(T_Z^1)$ are then given by:

$$T_Z^1 = \begin{cases} T - T_0 & T > T_0 \\ T + T_{\max} - T_0 & T \leq T_0 \end{cases} \quad (2)$$

A PEH data set is obtained by extracting data from the first maximum $Z_{\max}^1 = Z_i^1 > Z_{i+1}^1$, recording successively closer events $(Z_i^1, T_{Z,i}^1)$ satisfying the condition $Z_{i+1}^1 < Z_i^1$ for $Z_i^1 \geq Z_{\max}^1$.

5 THEORETICAL FRAMEWORK

5.1 GRB Flux and luminosity relations

We firstly define an isotropic equivalent photon luminosity in the source frame as:

$$L = \int_{1\text{keV}}^{10000\text{keV}} S(E)dE, \quad (3)$$

where $S(E)$ is the differential rest-frame source luminosity (in $\text{ph s}^{-1} \text{keV}^{-1}$). To define the observed peak photon flux (photons per cm^2 per second) observed within a detector band $E_{\min} < E < E_{\max}$ and emitted by an isotropically radiating source at redshift z one must perform two modifications. Firstly, the observed photon flux is modified to account for the missing fraction of the gamma ray energy seen in the detector band $b =$

$\int_{E_1}^{E_2} S(E)dE / \int_1^{10000} S(E)dE$. Secondly a cosmological k -correction, $k(z) = \int_{E_1}^{E_2} S(E)dE / \int_{E_1(1+z)}^{E_2(1+z)} S(E)dE$ is applied. With these two modifications the standard definition for flux becomes:

$$P = (1+z) \frac{L}{4\pi d_L(z)^2} \frac{b}{k(z)}. \quad (4)$$

Substituting in for b and $k(z)$ one obtains the familiar relation:

$$P = \frac{(1+z) \int_{(1+z)E_{\min}}^{(1+z)E_{\max}} S(E)dE}{4\pi d_L(z)^2}, \quad (5)$$

where $d_L(z)$ is the luminosity distance. The $(1+z)$ factor is included as the standard definition of $d_L(z)$ is valid for an energy flux, but P here is given as a photon flux (Mészáros et al. 2011). For long duration GRBs the function $S(E)$ is typically modeled by a Band function (Band 2003) which we use with high and low energy spectral indices of -2.25 and -1 and a break energy of 511 keV.

5.2 GRB Luminosity Function

A number of different forms have been suggested for the LGRB Luminosity Function (LF). To minimise our free parameters we use the single power law form used by Porciani & Madau (2000) which has an exponential cutoff at low luminosity:

$$\Phi(L) = \Phi_0 \left(\frac{L}{L_*} \right)^{-\alpha} \exp\left(-\frac{L}{L_*}\right). \quad (6)$$

Here, L is the peak rest frame photon luminosity in the 1-10000 keV energy range, α ensures an asymptotic slope at the bright end and L_* is a characteristic cut-off scaling. The normalisation coefficient for this LF is given by $\Phi_0 = [L_* \Gamma(\alpha - 1)]^{-1}$. Based on the studies of Meszaros & Meszaros (1996, 1995); Reichart & Meszaros (1997); Butler et al. (2010) we will assume no luminosity evolution with redshift.

5.3 GRB rate evolution

To model GRB rate evolution, $R_{\text{GRB}}(z)$, we assume that LGRBs track the star formation history of the Universe (Mészáros et al. 2006) and normalise a star formation rate model, $R_{\text{SF}}(z)$, (in units of mass converted to stars per unit time and volume) to the local ($z = 0$) rate. Multiplying by the local rate density ρ_0 (in $\text{Gpc}^{-3} \text{yr}^{-1}$) allows one to extrapolate rate evolution to cosmological volumes:

$$R_{\text{GRB}}(z) = \rho_0 \frac{R_{\text{SF}}(z)}{R_{\text{SF}}(z=0)}. \quad (7)$$

For $R_{\text{SF}}(z)$ we use the model of Li (2008), which was obtained by adding ultraviolet and infrared measurements to the sample of Hopkins & Beacom (2006). This takes the form:

$$R_{\text{SF}}(z) = \frac{(0.02 + 0.12z)}{1 + (z/3.23)^{4.66}}. \quad (8)$$

A number of studies suggested that cosmic metallicity evolution must also be considered in any rate evolution model for LGRBs (Li 2008; Modjaz et al. 2008). A metallicity dependence results from the requirement that

Wolf-Rayet (WR) stars should retain sufficient rotation to power a GRB – therefore angular momentum losses through stellar-wind induced mass-loss must be minimized (Woosley & Heger 2006). As wind-driven mass loss in WR stars is understood to be dependent on a high enough fraction of iron, a low-metallicity environment is an essential requirement (Vink & de Koter 2005; Woosley & Janka 2005).

Recent results from Elliott et al. (2012), driven by observations of LGRBs in metal rich galaxies, suggest that interpretations of luminosity and metallicity evolution could simply result from a misunderstanding of various redshift biases (Coward et al. 2008). As we will demonstrate later in section 9, the methods employed in this paper are sensitive to the rarer low- z population of bursts. Therefore, for clarity, and in support of the uncertainties discussed above, we will ignore the effects of metallicity evolution in this study.

5.4 The all sky event rate equation of GRBs

The number of GRBs per unit time within the redshift shell z to $z + dz$ with luminosity L to $L + dL$ is given by:

$$\frac{dN}{dt dz dL} = \psi(z) \frac{dV(z)}{dz} \frac{R_{\text{GRB}}(z)}{(1+z)} dz \Phi(L). \quad (9)$$

Here the $(1+z)$ factor accounts for the time dilation of the observed rate by cosmic expansion; its inclusion converts source-count information to an event rate. The co-moving volume element:

$$\frac{dV}{dz} = \frac{4\pi c}{H_0} \frac{d_L^2(z)}{(1+z)^2 h(z)}, \quad (10)$$

describes how the number densities of non-evolving objects locked into Hubble flow are constant with redshift. The quantity $h(z)$, is the normalized Hubble parameter,

$$h(z) \equiv H(z)/H_0 = [\Omega_m(1+z)^3 + \Omega_\Lambda]^{1/2}, \quad (11)$$

where $\Omega_m + \Omega_\Lambda = 1$ (for further details see Carroll et al. 1992). For a ‘flat- Λ ’ cosmology, we take $\Omega_m = 0.3$, $\Omega_\Lambda = 0.7$ and $H_0 = 72 \text{ km s}^{-1} \text{ Mpc}^{-1}$ for the Hubble parameter at the present epoch.

6 THE OBSERVATION-TIME RELATION FOR PEAK FLUX AND REDSHIFT

6.1 The $\log P$ – $\log T$ relation

From equation 9, the rate of GRBs with a peak photon flux greater than P observed by an instrument with sky coverage Ω is given by:

$$\dot{N}(> P) = \frac{\Omega}{4\pi} \int_{L_{\min}}^{L_{\max}} \Phi(L) dL \int_0^{z_{\max}(L,P)} \frac{dV(z)}{dz} \frac{R_{\text{GRB}}(z)}{(1+z)} dz, \quad (12)$$

were $z_{\max}(L, P)$ is the maximum redshift from which a burst with luminosity L and peak flux P can be detected.

To introduce an observation-time dependence, T , we follow the probability event horizon concept of Coward & Burman (2005) and note that as GRBs are independent of each other their observation-times will follow a Poisson distribution in time. Therefore, the temporal separation between events will follow an exponential distribution

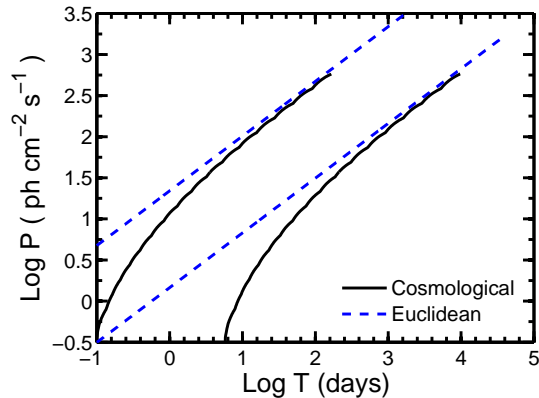


Figure 3. Cosmological and Euclidean $\log P$ – $\log T$ curves. The two curves converge at high observation-times.

defined by a mean number of events, $\dot{N}(> P)T$. The probability ϵ for at least one event $> P$ is given by:

$$\mathcal{P}(n \geq 1; \dot{N}(> P), T) = 1 - e^{-\dot{N}(> P)T} = \epsilon. \quad (13)$$

For this equation to remain satisfied with increasing observation-time:

$$\dot{N}(> P)T = |\ln(1 - \epsilon)|. \quad (14)$$

Equating the above equation for P and T we obtain a relation for the evolution of peak flux as a function of observation-time. By setting ϵ to some arbitrary value, $\log P$ – $\log T$ curves can be obtained numerically through equations 12 and 14.

Assuming a constant radial distribution of sources, Howell et al. (2007b) derived the following compact form for a $\log P$ – $\log T$ relation, which is a $T^{2/3}$ power law for a Euclidean distribution of sources:

$$P(T) = T^{2/3} \left(\frac{\Delta\Omega r_0}{3\sqrt{4\pi} |\ln(1 - \epsilon)|} \right)^{2/3} \left[\int_{L_{\min}}^{L_{\max}} \Phi(L) L^{3/2} dL \right]^{2/3}. \quad (15)$$

Figure 3 compares both the cosmological (equations 12 and 14) and Euclidean (equation 15) curves for arbitrary parameters of source evolution and LF. Following Howell et al. (2007a) we have plotted upper and lower thresholds by setting $\epsilon = (0.95; 0.05)$ – we will refer to these curves as 90% PEH thresholds. We note that as observation-time increases the Euclidean and Cosmological curves begin to converge. This represents the increased probability of obtaining a cosmological bright event from the bright $-3/2$ power law part of the $\log N$ – $\log P$ distribution. The Euclidean curves are convenient in that they can provide initial estimates by fitting to the brightest sample of PEH peak flux data.

6.2 The $\log Z$ – $\log T$ relation

One can extend the arguments of the previous section to derive a $\log Z$ – $\log T$ relation. From equation 9 the rate of GRBs observed by an instrument with sky coverage Ω within a redshift limit Z_L is given by:

$$\dot{N}(< Z_L) = \frac{\Omega \eta_z}{4\pi} \int_{L_{\min}(P_L, Z_L)}^{L_{\max}} \Phi(L) dL \int_0^{Z_L} \frac{dV(z)}{dz} \frac{R_{\text{GRB}}(z)}{(1+z)} dz, \quad (16)$$

with z_L obtained by applying the flux limit of the detector, P_L , to equation 5. The quantity η_z is the efficiency of obtaining a redshift, approximated as the fraction of the total burst sample with measured redshifts. Using a similar argument as used to determine equation 14, one obtains the following relation for the temporal evolution of redshift:

$$\dot{N}(< Z_L)T = |\ln(1 - \epsilon)|. \quad (17)$$

This equation can be equated for T and z to set a spatial dependence on GRB populations. Curves of $\log Z - \log T$ for $\epsilon = (0.95; 0.05)$ can be obtained numerically through equations 16 and 17.

By using a single $\log Z - \log T$ curve as a threshold Coward & Burman (2005) showed that SL-GRBs appeared as outliers, supporting the suggestion that they were a sub-population of classical LGRBs. In this paper we have extended their relation, based solely on the cosmological event rate evolution $R_{\text{GRB}}(z)$, to include the effects of detector sensitivity and the luminosity distribution of sources. As shown above, this allows the $\log Z - \log T$ relation to be derived seamlessly from a standard integral distribution. Thus, model parameters obtained by fitting to a differential brightness distribution should satisfy the two observation-time relations presented above (equations 14 and 17). This circumvents a difficulty encountered in previous studies which fitted directly to the PEH data to determine a rate – the resulting rate estimates had low resolution due to the intrinsic scatter of PEH data (Howell et al. 2007a; Howell et al. 2010).

Before we go on to apply the fits described in sections 6.1 and 6.2 to PEH data, we will first determine the parameter values that will be used in the models of $\log(P; Z) - \log T$. We will do this by fitting our data to the brightness distribution of GRBs.

7 FITTING TO THE GRB BRIGHTNESS DISTRIBUTION

In this section we perform χ^2 minimisation of the brightness distribution of both *Swift* and BATSE LGRBs to obtain values for the three free parameters ρ_0 , L_0 and α . A goodness of fit for this procedure is obtained by dividing the minimised χ^2 value by the number of degrees of freedom, χ^2/dof . We note that although the $\log(P; Z) - \log T$ relations are derived from an integral distribution, we fit to a differential distribution in which the number of sources are independent at each interval of $P + dP$ ⁴. From equation 9 one can define a differential $\log N - \log P$ relation (Kommers et al. 2000; Porciani & Madau 2000; Salvaterra & Chincarini 2007; Campisi et al. 2010) which is

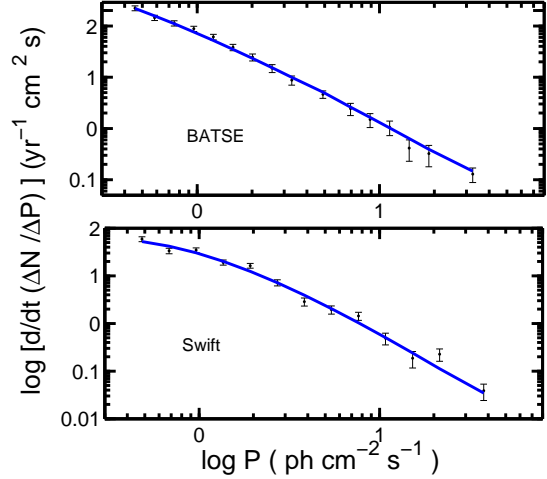


Figure 4. The differential $\log N - \log P$ distribution of BATSE (top) and *Swift* (bottom).

the observed rate of bursts within a peak flux interval (P_1 , P_2) as:

$$\dot{N}(P_1 \leq P < P_2) = \frac{\Omega}{4\pi} \int_0^\infty \frac{dV(z)}{dz} \frac{R_{\text{GRB}}}{(1+z)} dz \int_{L(P_1, z)}^{L(P_2, z)} \Phi(L) dL, \quad (18)$$

with $L(P_{1,2}, z)$ obtained through equations 4 and 5.

We bin peak flux data into logarithmical spaced intervals ΔP and ensure each bin contains at least 5 bursts (Wall et al. 2003). Bursts per bin ΔN and their uncertainties $\pm \sqrt{\Delta N}$ are converted into burst rates ΔR by dividing by the live time of the search ΔT (Kommers et al. 2000).

7.1 The BATSE $\log N - \log P$ distribution

A number of studies have utilized the Kommers et al. (2000) differential peak flux distribution data (eg. Porciani & Madau 2000; Salvaterra & Chincarini 2007; Campisi et al. 2010). As we require both the discrete peak flux values and their observation-times to produce a $P(T)$ distribution in the next section, we make our own data selection from the BATSE current catalogue⁵. We note however, the Kommers et al. (2000) sample is a good consistency test for our models and we find good agreement using the best fit parameters of (Porciani & Madau 2000; Salvaterra & Chincarini 2007).

The BATSE instrument performed a number of runs at different trigger energy ranges and photon count rate thresholds throughout its operation. These runs, in effect, represented different experiments⁶. For consistency, we condition this data by selecting bursts from the (50–300) keV band obtained when the trigger thresholds were set to 5.5σ . Following Guetta et al. (2005) and Guetta & Piran (2007) we additionally select bursts for which the ratio of count rates, C , at the 1024 ms timescale $C_{\max}/C_{\min} \geq 1$ – here

⁵ <http://www.batse.msfc.nasa.gov/batse/grb/catalog/current/>

⁶ For example, during the first 17 months of operation the energy range was set to (50-300)keV, although the trigger thresholds were varied.

⁴ Bright objects will contribute to counts at all values of P in an integral distribution

Data	Trigger numbers	Number of bursts	Run time (days)
A	105–178	11	18
B	268–1851	164	437
C	1928–3175	198	724
D	3883–3941	14	41
E	5403–5519	37	76
F	6102–6764	143	448
G	7356–7767	29	228

Table 1. The BATSE data segments of bursts that triggered in the (50–300) keV band when the trigger thresholds were set to 5.5σ . We show the number of bursts within each segment that passed our selection criteria and the instrument run time associated with each segment.

C_{\max} is the rate in the second brightest detector. We finally select long bursts with $T_{90} > 2s$ and with set a threshold of $P_{\min} = 0.4$ corresponding to the value at which the triggering algorithm is almost 100% efficient (Paciesas et al. 1999). We find that 596 GRBs meet these criteria.

Table 7.1 summarizes the different data segments and the total number of bursts meeting the above constraints. We show the trigger numbers (rather than the dates) and the total detector run time to form each segment. In our later analysis we will apply the $\log P - \log T$ method to both the combined data and to the largest of the individual segments.

Figure 4 (top panel) shows the best fitting results to the BATSE differential peak flux distribution using $\Omega = 0.67\pi$ and a live time of $\Delta T = 3.19$ yr. The peak flux intervals, number of bursts and burst rates data used for the fit are given in Table A1. We find a best fit of $\rho_0 = 0.12^{+0.1}_{-0.01} \text{Gpc}^{-3} \text{yr}^{-1}$, $L_* = 3.1^{+364}_{-1.7} \times 10^{51} \text{ergs}^{-1}$ and $\alpha = -2.2^{+0.17}_{-0.32}$. The goodness of fit is given as $\chi^2/dof = 6.6/13 \sim 0.51$.

7.2 The *Swift* $\log N - \log P$ distribution

In recent studies Zhang (2011) and Bromberg et al. (2012) have suggested that the $T_{90} = 2s$ division of short and long GRBs based on the BATSE bimodal distribution (Kouveliotou et al. 1993) is a detector dependent categorisation and therefore not appropriate for *Swift* bursts. Other studies have suggested an intermediate duration class of bursts between these two classes (Horváth et al. 2010b). For our LGRB sample, we obtain peak flux values from the *Swift* online catalogue⁷ but rather than employing a T_{90} cut, we use the categorisations given in the Jochen Greiner online catalogue (JG) of well localized GRBs⁸. As the burst categorisations in this catalogue are subject to review through follow up observations we find it a useful resource to obtain our LGRB sample. We find that from the *Swift* peak flux sample of 649 bursts up to burst 120224A, 644 are categorised in the JG catalogue. We exclude the three SL-GRBs, 060218, 060505 and 100316D (see section 10.1 for further discussion of these bursts) and 12 bursts categorised as SGRB-EE (all but one have $T_{90} > 2s$) (Norris et al. 2011). We follow Guetta & Piran

(2007), Wanderman & Piran (2010) and Salvaterra et al. (2009) and adopt a simplified approach to account for detector sensitivity by applying a peak flux cut at $0.4 \text{ ph sec}^{-1} \text{ cm}^{-2}$ leaving a total sample of 555 LGRBs.

Figure 4 (lower panel) shows the best fitting results to the *Swift* differential peak flux distribution. The peak flux intervals, number of bursts and burst rates data used for the fit is given in Table A2. We find best fit results of $\rho_0 = 0.09^{+0.01}_{-0.01} \text{Gpc}^{-3} \text{yr}^{-1}$, $L_* = 2.0^{+0.2}_{-0.02} \times 10^{52} \text{erg s}^{-1}$ and $\alpha = -3.8^{+0.2}_{-0.6}$ with a goodness of fit $\chi^2/dof = 19.9/10 \sim 2$. These values are in agreement with the no-evolution model of Salvaterra & Chincarini (2007).

8 THE $\log P - \log T$ DISTRIBUTION OF LGRBS

In this section we apply the estimated parameters, L_* , α and ρ_0 to the 90% PEH $\log P - \log T$ thresholds given in section 6.1 and attempt to constrain peak flux PEH data.

As a distant bright burst could produce a similar peak flux as a closer burst of moderate brightness, an intrinsic scatter will be present in $P(T)$ data. This, in combination with the spatial distribution of bursts, means it is difficult to use a 90% $\log P - \log T$ threshold to separate burst populations. The spatial dependence introduced in section 6.2 will provide a stronger case for untangling burst populations. The goal of this section is two fold: a) to show that the parameters obtained using the $\log N - \log P$ fits are compatible and complementary with the $\log P - \log T$ relation; b) to demonstrate how data conditioning methods improve the quality and quantity of the PEH data.

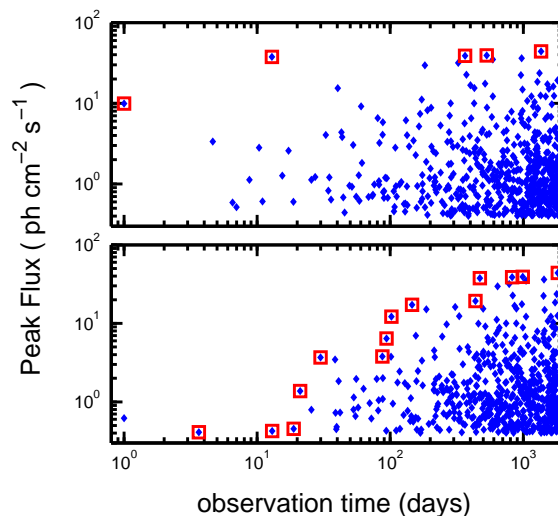


Figure 5. The top panel shows the BATSE $P(T)$ sample obtained by chronologically combining the data sets A-F of table 7.1. The bottom panel shows the same data after applying the FromMAX algorithm to temporally re-ordering the data from the maximum peak flux. The PEH data are indicated in each panel by squares. The top panel illustrates how an energetic event occurring at early observation-time can decrease the PEH sample. The bottom panel shows how some simple processing using FromMAX can circumvent this problem.

⁷ http://swift.gsfc.nasa.gov/docs/swift/archive/grb_table/

⁸ <http://www.mpe.mpg.de/~jcg/grbgen.html>

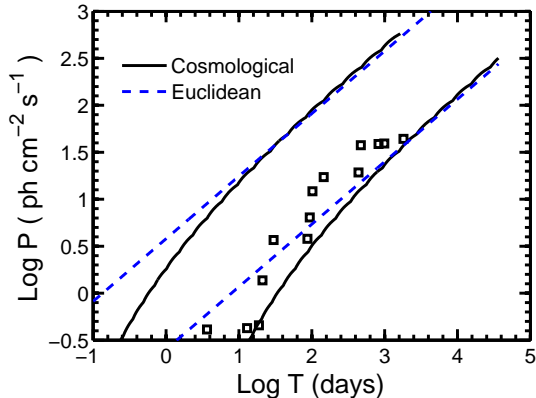


Figure 6. The $\log P$ – $\log T$ data of Figure 5 is constrained using cosmological 90% PEH curves. At high observation-time the data is also constrained by a Euclidean model.

8.1 The BATSE $\log P$ – $\log T$ distribution

The $\log P$ – $\log T$ method can be used to fit to either the individual data runs of BATSE shown in Table 7.1 or a combined set – this allows several consistency tests of the method. We firstly use all the available data to construct a single time series $P(T)$ by chronologically combining the 6 data sets A-F. A temporal dependence is obtained by adding the observation-times of the j th data set T_j to the maximum of the previous $\max(T_{j-1})$. When joining two consecutive data sets an additional factor of $T = 1.5$ days, the mean time between events for BATSE, is also added to the first event of T_j to ensure a sufficient delay time is included.

Figure 5 shows the combined BATSE $\log P(T)$ data. The top panel shows the pre-processed sample with PEH data shown by squares. We see that as observation-time increases, so too does the probability of a large event. The plot also illustrates how a bright event can occur near the start of a $P(T)$ time-series (at around 10 days) and thus minimise the PEH sample - we will see later that this effect can also be seen in the individual data sets A-F.

The bottom panel of Figure 5 shows the same data after applying the fromMAX technique to temporally re-order the data from the brightest event (as described in section 4). The advantage of the fromMAX method is clearly illustrated – the PEH sample is increased from 5 events to 14 events.

To test that PEH data set obtained through FromMAX (top panel) is statistically compatible with that obtained from the pre-conditioned data (top panel), we apply a 2D-Kolmogorov-Smirnov test (2DKS) (Peacock 1983; Fasano & Franceschini 1987) and obtain a KS probability of 29% showing the two samples are statistically consistent.

Figure 6 shows the 90% $\log P$ – $\log T$ thresholds and peak flux PEH data of BATSE. We see that the data is well constrained by the cosmological threshold. In addition to the increased size of the sample, the improvement obtained using the FromMAX method can be further validated through binomial maximum likelihood (BML) estimates for obtaining data within the 90% thresholds. We find a BML of 92% for the data shown in Figure 6 (1 failure in 14). We find a BML of 60% for the pre-processed PEH data shown in the top panel of Figure 5 (2 failures in 5). We note that a bias towards the lower threshold ($\epsilon = 95\%$) is evident - this is a

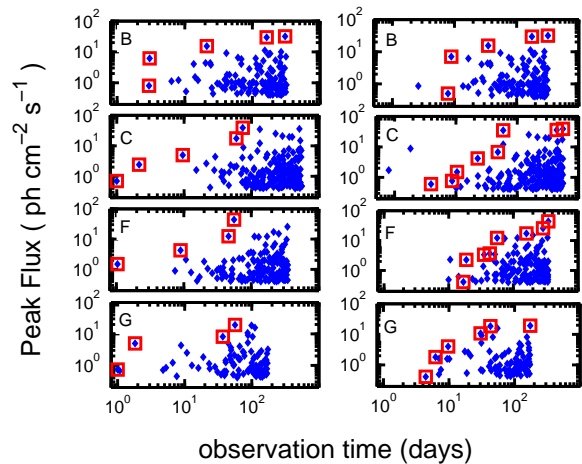


Figure 7. As for Figure 5 but this time showing on the left PEH data from pre-processed $P(T)$ samples B,C,F and G. The FromMAX PEH data from each sample is shown on the right. We see that the sample size is increased in all but the first case.

result of the data conditioning rather than an intrinsic bias, as will become apparent when we next apply the method to individual data sets.

Figure 7 shows a repeated analysis for the 4 largest individual data segments, B,C,F and G. The left sided panels display the pre-processed data (PEH data is again shown by squares) and the right sided panels show the time series after applying the FromMAX method. We see that the PEH data has increased in 3 of the 4 samples.

Figure 8 shows the 90% $\log P$ – $\log T$ thresholds applied to the 4 sets of PEH data shown in the right hand panels of Figure 7. The plot shows that the PEH data is again well constrained. The bias towards the lower threshold ($\epsilon = 95\%$) evident in Fig. 6 is only apparent for data set F, suggesting that this is a manifestation of the data conditioning rather than the BATSE sample. The plot does suggest that methods such as data splitting and recombining procedures as used in Howell et al. (2007a) on simulated data could prove useful to increase PEH data sets from long time-series.

Table 2 compares the amount of PEH data and the BML estimations obtained using the 4 sets of pre-processed data with those obtained after applying the FromMAX method. All cases show that the amount of PEH data and/or the BML estimates have improved from the processing. Additionally, the 2DKS probabilities are given, which all indicate good statistical compatibilities between the pre-processed PEH samples and after applying FromMAX.

8.2 The Swift $\log P$ – $\log T$ distribution

Figure 9 shows the *Swift* FromMAX time-series – the pre-processed $P(T)$ data was shown previously in Fig. 1. In comparison to BATSE sample shown in the top panel of Fig. 5, one could argue that the *Swift* data already seems well conditioned to extract PEH data. This is because: a) the largest event in the the pre-processed *Swift* data occurred near the end of the observation-time; b) no significantly bright event has occurred at early observation-time.

Figure 10 shows the 90% $\log P$ – $\log T$ thresholds using both the pre-processed and FromMAX time-series. Both PEH samples recorded BML values of 100% although the

Data set		B	C	F	G
Pre-conditioned PEH data	Size	5	5	4	4
	BML	80%	100%	100%	75%
FromMAX PEH data	Size	5	8	8	6
	BML	100%	100%	88%	100%
2DKS Probability		0.84	0.85	0.68	0.28

Table 2. A comparison of PEH data obtained from pre-conditioned data with that obtained using the FromMAX method. The table shows that the amount of data and/or binomial maximum likelihood (BML) estimates improve with the FromMAX method. A 2D Kolmogorov-Smirnov test on the two PEH samples from each data set shows that the statistical PEH signature is not lost by using the FromMAX method.

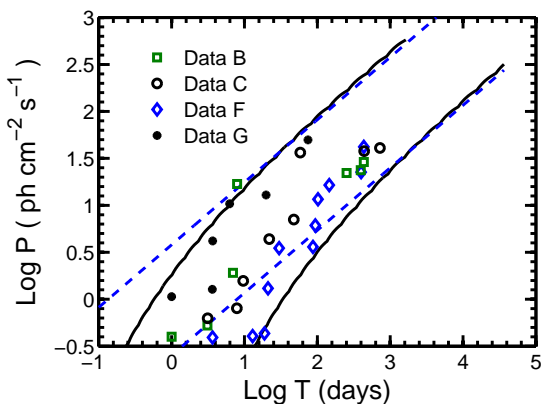


Figure 8. As for Figure 6 but with the PEH data of Figure 7 obtained using FromMAX. We see that the PEH data is well constrained by the 90% $\log P - \log T$ thresholds.

FromMAX method has produced an increase in data. The statistical compatibility between the PEH samples before and after applying FromMAX is confirmed by a value of 0.46.

We have shown in this section that a $\log P - \log T$ distribution of GRBs is in agreement with a $\log N - \log P$ distribution and that the method can be applied to data sets obtained from different detectors. We have further shown

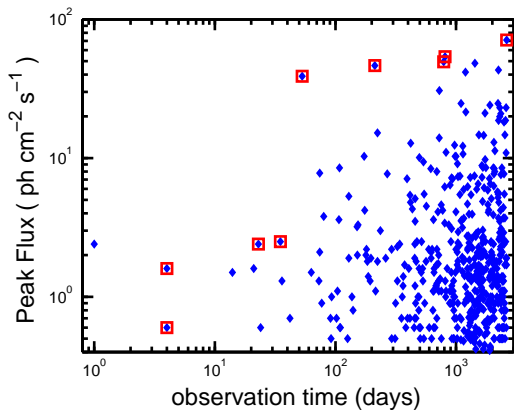


Figure 9. The $P(T)$ distribution of *Swift* after applying the FromMAX method.

how some processing can improve the quality and quantity of data. In the next section we shall apply the same principles to the redshift domain and will show how the technique can be used to differentiate between different populations of burst.

9 THE SWIFT LOG $Z - \log T$ DISTRIBUTION

As discussed earlier, the PEH sample of a $Z(T)$ distribution approaches the low- z regime rapidly (Coward & Burman 2005), thus the $\log Z - \log T$ method is most sensitive to the closest occurring events. The dependence on only the closest events mean that selection effects such as the ‘redshift desert’ (Coward et al. 2008) can be ignored. Additionally, as the source rate evolution is reasonably well predicted within $z \sim 2$ the choice of SFR model will not change the curves significantly. For the closest events, as redshift determinations would be expected to be more accurate, we include values obtained through all methods: absorption, emission and photometrically.

Figure 11 illustrates how the high- z variations have minimal influence on the $\log Z - \log T$ curves by examining the redshift selection function. The top panel shows the function $\dot{N}(< Z_L)$ defined by equation 16 assuming $P_L = 0.4$ – one may recall that $\log Z - \log T$ curves are produced by introducing a temporal dependence (equation 17). The dashed line shows the same function without the factor $S(L) = \int_{L_{\min}(P_L, z)}^{L_{\max}} \Phi(L) dL$ which can be referred to as a detector dependent scaling factor (see eq. 1 of Coward et al. 2008). The plot shows that this function has little effect until $z \sim 3$ ($z \sim 2$ for the BATSE instrument) – as the detection threshold decreases this value of z increases.

The lower panel shows the $\log Z - \log T$ for these two scenarios showing that there is little change in the two curves. Therefore one can make reasonable estimates without an accurate description of the luminosity distribution of the sources. For a $\log Z - \log T$ function, the rate density is the dominant variable. As such, one can discriminate between transient populations of different rate density solely by their spacial dependence.

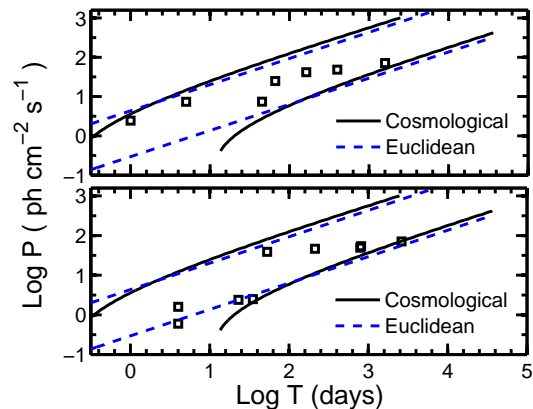


Figure 10. The 90% $\log P - \log T$ thresholds for *Swift* are used to constrain PEH data. Top panel - PEH data from the pre-processed time-series. Bottom panel - PEH data using the FromMAX time-series.

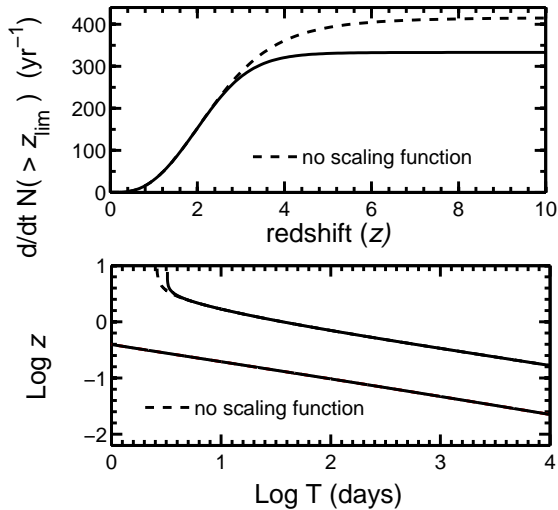


Figure 11. The top panel shows the function $\dot{N}(< Z_L)$ with and without the scaling factor discussed in the text. The lower panel shows that the two $\log Z - \log T$ curves differ little and are dependent only on the closest events of a source population.

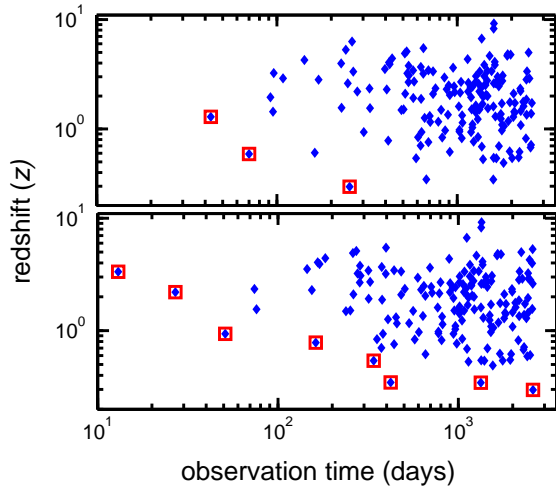


Figure 12. The *Swift* $Z(T)$ distribution with PEH data indicated by squares. The top panel shows the pre-processed sample. The lower panel shows the PEH data has increased after applying the FromMIN procedure.

Figure 12 shows the *Swift* $Z(T)$ distribution with PEH data indicated by squares. The *Swift* $Z(T)$ sample of 173 bursts is obtained by taking bursts from the selection of section 7.2 with certain redshift measurements. The data is given in Table B1. The top panel shows the pre-processed data and the lower panel shows the data after applying the FromMIN procedure described in section 4. The Figure shows that the PEH data set has been increased by applying FromMIN (the PEH data is indicated by bold in Table B1).

Figure 13 shows that the PEH data is well constrained by the 90% $\log Z - \log T$ thresholds. To account for the Swift efficiency in obtaining a redshift, ρ_0 is scaled by a factor of 0.3 to account for the number of bursts with redshifts (172) from our overall sample (576). To test the compatibility of the PEH data obtained using the FromMIN method with that obtained from the pre-processed $Z(T)$ we perform

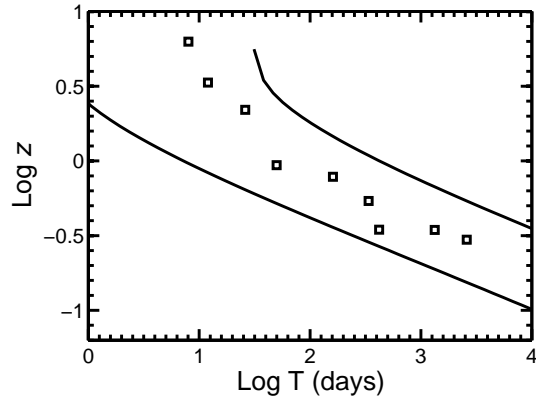


Figure 13. The 90% $\log Z - \log T$ thresholds and PEH data for the *Swift* LGRB sample obtained using the FromMIN method. The data is well constrained using the rate $\rho_0 = 0.09^{+0.01}_{-0.01} \text{Gpc}^{-3} \text{yr}^{-1}$ estimated through a $\log N - \log P$ fit.

a 2DKS test. A probability of 0.87 indicates that the two samples are from the same distribution.

We have shown in this section by extracting PEH data from the *Swift* $Z(T)$ sample that the $\log Z - \log T$ relation is in good agreement with both the $\log N - \log P$ and $\log P - \log T$ relations. We have also illustrated that a $\log Z - \log T$ distribution relies strongly on the spacial distribution of the sources and is invariant to the detector selection function. In the next section we will demonstrate how the method can differentiate between source populations.

10 THE $\log Z - \log T$ RELATION APPLIED TO SL-GRBS

10.1 The $\log Z - \log T$ relation as a prob of burst populations

In this section we will demonstrate that the $\log Z - \log T$ method can be used to differentiate between different source populations. A key principle we will use is that PEH data represents the rarer, brighter or closer events that are less subject to detector selection bias. Thus, insight into the average properties of a source population can be provided from only a small sample of PEH events.

Bursts from the same distribution, with the same intrinsic rate density, should produce PEH data that is constrained by a $\log Z - \log T$ threshold. A separate burst population, occurring at a higher rate, will produce rarer PEH events at earlier observation-times and visa-versa for populations at lower rates. For two mixed $Z(T)$ populations, their observation-time sequence will differ, thus producing outlying events to a 90% $\log Z - \log T$ threshold.

10.2 The *Swift* sub-luminous GRB sample

In addition to the two excepted SL-GRBs in the *Swift* sample, GRB 060218 and GRB 100316DA, a number of other candidates have also been discussed. Based on their low luminosities and subsequent Poisson detection probabilities, Wanderman & Piran (2010) suggested three additional bursts could contribute to the SLGRB popula-

GRB	F_{peak} $\text{ph s}^{-1}\text{cm}^2$	T_{90} s	T days	L_{iso} erg s^{-1}	α	z
060218	0.25	2100	427	1.4×10^{47}	-2.3	0.03
060505	2.65	4	504	9.1×10^{48}	-1.3	0.089
100316D	0.1	1300	1915	4.8×10^{47}	-2.3	0.059

Table 3. Data for the three *Swift* sub-luminous bursts. The isotropic rest frame (1-10000 keV) luminosities are obtained from the peak luminosity values (ph s^{-1}) using a simple power law fit with values of α taken from the *Swift* online catalogue.

tion: GRB 050724, GRB 051109 (see also Bromberg et al. 2012) and GRB 060505. Of these three bursts we include GRB 060505 in our sample. Although GRB 050724 was a long duration burst ($T_{90} \sim 96$ s), further analysis has suggested that it is of the SGRB category (Campana et al. 2006; Grupe et al. 2006; Malesani et al. 2007)– most likely a SGRB-EE (Norris et al. 2010, 2011). GRB 051109 is also omitted due to uncertainty in the redshift estimation⁹ (in accordance with our selection criteria of section 12).

Despite GRB 060505 being relatively nearby and well observed, intense photometric and spectroscopic searches found no evidence of an associated supernova despite the fact an event ~ 100 times fainter than SN 1998bw would have been detected (McBreen et al. 2008; Xu et al. 2009). Dust obscuration was excluded for this burst and Fynbo et al. (2006) and Ofek et al. (2007) argued that the simplest explanation was that GRB 060505 was simply the closest observed SGRB. Other studies however found the properties of the host galaxy consistent with that of the LGRB class (Ofek et al. 2007; Thoene & Fynbo 2007; Thöne et al. 2008). Furthermore, McBreen et al. (2008) showed the spectral lag was consistent with that of a LGRB¹⁰ and an extensive study of the afterglow performed by Xu et al. (2009) found afterglow parameters within the range for other LGRBs. In view of its luminosity, we include this burst from our analysis of SL-GRBs in the next section. However, to further address the classification of this burst, we will investigate its compatibility to the Swift SGRB population in the final section. Table 3 shows the main parameters for these three SL-GRBs which will be used in the analysis of this section.

10.3 The $\log Z - \log T$ analysis of *Swift* SL-GRBs

Figure 14 shows the $P(T)$ time-series for the LGRB sample obtained using FromMIN and including the three SL-GRBs 060218, 060505 and 100316D. The PEH data are indicated by squares – the SL-GRB sample are clearly shown as significantly close events. On inspection, GRB 060505 stands out as a particularly rare event due to its occurrence at a relatively early observation-time.

Figure 15 shows the 90% $\log Z - \log T$ thresholds based on the LGRB parameters used in section 9 along with the PEH data. This plot clearly shows that the three SL-GRBs

⁹ A putative host galaxy at $z = 0.08$ was reported in GCN 5387 by D. A. Perley et. al.

¹⁰ LGRBs support the lagluminosity relation of Norris et al. (2000) while SGRBs have zero lag.

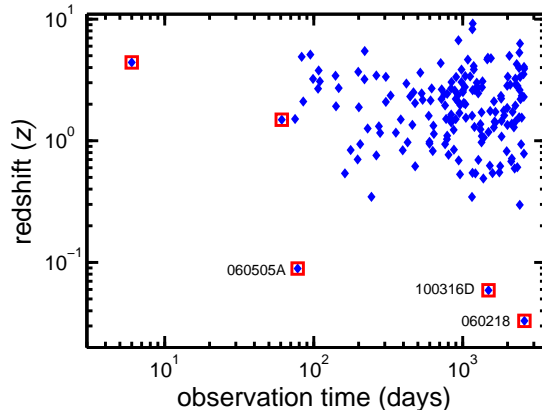


Figure 14. The $Z(T)$ time series for Swift LGRBs including three *Swift* SL-GRBs.

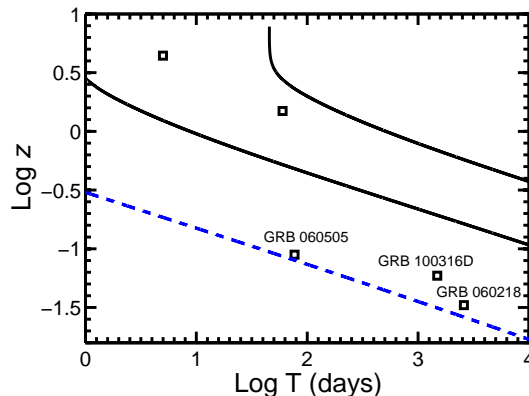


Figure 15. The $\log Z - \log T$ distribution for *Swift* LGRBs including three SL-GRBs which are labeled. The dashed line represents a 0.02% probability for obtaining a LGRB within redshift z at an observation-time T .

are outliers to the distribution suggesting they are from a population occurring at a higher rate. Based on the 90% thresholds of Fig. 13, assuming that the SL-GRBs are from the low-probability tail of the LGRB distribution, one would expect to wait 87 (1800) years to observe a burst as close as GRB 060505 (GRB 060218). The probability of observing these bursts at time T can be estimated by extending the PEH threshold upper limit through ϵ - this new limit is shown in Fig. 15 by the dashed curve. We find a probability value of $\epsilon = 0.00015$ is required to constrain the SL-GRB bursts at the LGRB rate. This value is consistent with that estimated by Coward (2005) for the probability of observing the low- z burst GRB 980425.

If the SL-GRB sample are from a distinct population one should be able to constrain them using separate 90% $\log Z - \log T$ thresholds set at a higher rate value $\rho_{0,SL}$ and a LF representative of the SL-GRB sample. For the LF we consider the form used for the LGRB sample but with $L_* = 10^{49} \text{ erg s}^{-1}$ which is around three orders of magnitude lower than that derived in section 7. As described in the previous section, consideration of $S(L)$ is not essential but is included for completeness. To estimate $\rho_{0,SL}$ for

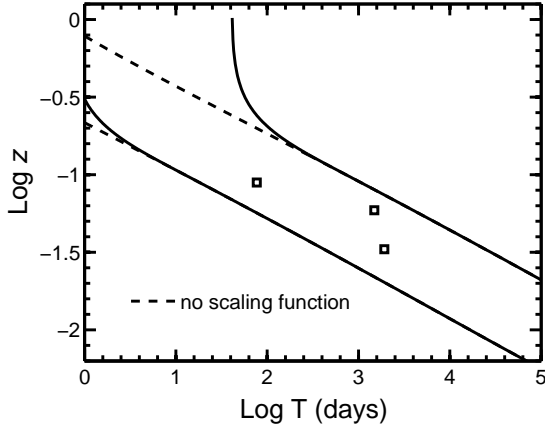


Figure 16. The $\log Z$ – $\log T$ distribution for *Swift* SL-GRBs.

the *Swift* SL-GRB sample we follow Guetta & Della Valle (2007); Coward et al. (2012) and calculate

$$\rho_{0,SL} = \sum_i^3 \frac{1}{V_{\max}} \frac{1}{T} \frac{1}{\Omega} \frac{1}{\eta_z} \quad (19)$$

Here V_{\max} is the maximum volume each burst could be detected, T is the maximum observation-time for the sample, Ω is the sky coverage and we assume $\eta_z = 0.3$ as for the LGRB sample. To determine V_{\max} we use equation 4 and assume a flux limit of 0.15 ph sec^{-1} – this corresponds with the detection threshold of 95% of the *Swift* LGRB sample. We obtain $\rho_{0,SL} = 147_{-92}^{+180} \text{ Gpc}^{-3} \text{ yr}^{-1}$ where the errors are the 90% Poisson confidence limits (Gehrels 1986). This rate, based solely on the *Swift* sample, is in agreement with other studies of the SL-GRB population (e.g. Coward 2005; Soderberg et al. 2006; Guetta & Della Valle 2007; Pian et al. 2006; Liang et al. 2007; Virgili et al. 2008; Howell et al. 2011)

Figure 16 shows the 90% $\log Z$ – $\log T$ thresholds corresponding to $\rho_{0,SL}$. To show that the $\log Z$ – $\log T$ method allows constraints to be made solely on $\rho_{0,SL}$, the dashed lines show the curves obtained without the selection function $S(L)$. The SL-GRB PEH data is well constrained demonstrating good agreement with the rate estimates and supporting the hypothesis of a distinct SL-GRB population of bursts. Additionally, the figure supports the hypothesis that GRB 060505 is a member of the SL-LGRB category.

10.4 Testing the connection between SL-GRBs and XRFs

We note that the two sub-luminous bursts GRB 060218 and GRB 100316D are often categorised as XRFs. Although XRFs are generally understood to represent the fainter and softer part of the GRB distribution (Zhang 2007; Sakamoto et al. 2008) the relation between XRFs and SL-GRBs is not clear. Looking at *Swift* data the durations of both GRB 060218 (2100s) and GRB 060218 (1300s) are both much higher than those of other XRFs in the cat-

GRB	Peak Flux	redshift
101219A	4.1	0.718
100206A	1.4	0.4068
100117A	2.9	0.92
090510	26.3	0.903
070724A	2.03	0.457
061217	2.36	0.827
051221A	12	0.5465
050509B	3.71	0.226
080905A [†]	6.03	0.1218
060505*	2.65	0.089

Table 4. The *Swift* SGRB data sample. The lower two entries are investigated as members of the SGRB population: * possible SL-GRB but no SN observed to deep limits; [†] low- z outlier to the Yonetoku relation with high energy properties typical of a SGRB (see section 10.4).

alogue¹¹ suggesting that a different mechanism separates the two categories. It is therefore interesting to extend the $\log Z$ – $\log T$ analysis of the previous section to investigate the connection between SL-GRBs and XRFs using $Z(T)$ data. We find that including two XRFs with secure redshifts¹²: XRF 050416A ($z=0.65$) and XRF 050824 ($z=0.83$); does not change the result given in Figure 15. Our analysis using the *Swift* sample with secure redshifts therefore suggests that XRFs and SL-GRBs are from a different population.

10.5 A $\log Z$ – $\log T$ analysis of GRB 060505

Although the last section shows that based on a $\log Z$ – $\log T$ analysis, GRB 060505 is not of the LGRB category, the lack of an accompanying SN to stringent limits still suggests it could be of the SGRB class. A additional test is therefore to include this event in the $Z(T)$ distribution of *Swift* SGRBs and repeat the previous analysis.

To calculate the observed rate of SGRBs, $\rho_{0,S}$, we add GRB 060505 to the SGRB sample of Coward et al. (2012) and extend equation 19 through the factor $R_{B/S} = 6.7$ to account for the reduced sensitivity of *Swift* for detecting SGRBs in comparison to BATSE. We omit an anomalous burst GRB 080905A from our sample – a repeat analysis at the end of this section will consider this burst. Setting $\eta_z = 9/41$ we obtain $\rho_{0,S} = 8.57_{-7.7}^{+24.7} \text{ Gpc}^{-3} \text{ yr}^{-1}$.

Figure 17 shows the 90% $\log Z$ – $\log T$ thresholds including GRB 060505, which is shown as a clear outlier. We find that a value of $\epsilon = 0.007$ is required to constrain this burst indicating a $> 99\%$ probability that a SGRB would not have occurred at $z = 0.09$. Our analysis therefore suggests that GRB 060505 belongs in the SL-GRB sample of bursts.

The previous analysis excluded the burst GRB 080905A. This spectrally hard, short duration burst ($T_{90} = 1 \text{ s}$) showed negligible spectral lag, no evidence of extended

¹¹ Of the 11 XRFs in the *Swift* data up to January 2012 the longest T_{90} is 103s; 6 have durations below 10s.

¹² As in section 7.2 we again base our categorisations and redshifts on the Jochen Greiner online catalogue.

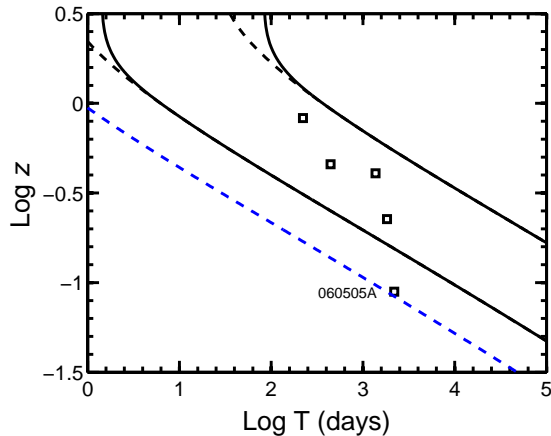


Figure 17. The $\log Z - \log T$ distribution for Swift SGRBs showing that GRB 060505 is an outlier to this distribution. The dashed curve indicates a $> 99\%$ probability that a SGRB would not have occurred at $z = 0.09$.

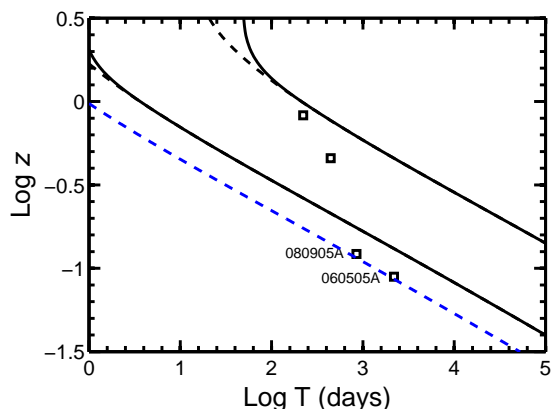


Figure 18. As for Fig. 17 but including the burst GRB 080905A. We see that this burst, as well as GRB 060505 are outliers. The dashed curve indicates a $\sim 1\%$ probability that GRB 080905A could have occurred at $z = 0.12$.

emission or of an associated SN to deep limits – all properties of a SGRB resulting from a compact object merger. It was spectroscopically associated with a galaxy at redshift $z = 0.1218$ making it the closest possible SGRB (Rowlinson et al. 2010; Kann et al. 2011).

Figure 18 shows the result of a repeated analysis of GRB 060505 including GRB 080905A with 90% $\log Z - \log T$ thresholds corresponding to a recalculated rate of $\rho_{0,S} = 13.5^{+39.1}_{-12.2} \text{Gpc}^{-3} \text{yr}^{-1}$. The plot shows that as well as GRB 060505, GRB 080905A is also an outlier to the 90% thresholds. This finding supports an analysis by Gruber & for the Fermi/GBM collaboration (2012) which found GRB 080905A to be a clear outlier to the Yonetoku, $E_{p,\text{rest}} - L_p$ relation (Yonetoku et al. 2004); but see also Borgonovo & Björnsson (2006). They found that GRB 080905A would require a redshift $z \sim 0.9$ to be consistent with the Yonetoku relation, suggesting that the host, a large almost face-on spiral galaxy, could be a foreground galaxy. Rowlinson et al. (2010) noted that the offset of the afterglow was large (18.5 kpc) but comparable to other SGRB locations, especially considering the relative size of the host.

Our analysis suggests a $\sim 1\%$ probability (indicated by the dashed curve) that GRB 080905A could have occurred at $z = 0.12$. Furthermore, in agreement with Gruber & for the Fermi/GBM collaboration (2012), we find that given a redshift of $z \sim 0.9$, this burst would be constrained by the $\log Z - \log T$ relation.

Given that the observed prompt properties of this burst are highly consistent with a SGRB and the redshift is reasonable secure, the above analysis is interesting and implies that this burst may deserve additional attention. It certainly further highlights the ability of the $\log Z - \log T$ method to select out bursts with anomalous properties from a given sample.

11 CONCLUSIONS

In this study we have shown how the redshift and peak-flux distributions of GRBs have an observation-time dependence and have derived two new relations from the standard integral distributions - the $\log P - \log T$ and the $\log Z - \log T$. We have shown how a PEH data set can be extracted from the redshift and peak-flux time series and constrained by 90% thresholds using the above two relations. We have demonstrated that the FromMIN and FromMAX methods improve the PEH data sample and circumvent a bias introduced by the occurrence early event.

By applying the $\log P - \log T$ method to both *Swift* and BATSE data we showed that the relation is in agreement with parameters obtained through a $\log N - \log P$ fit. We then showed that the same parameters could be used to constrain PEH data using a $\log Z - \log T$ relation. By including the Swift SL-GRB sample of bursts we showed that this sample were outliers to the LGRB sample and could be constrained by a 90% $\log Z - \log T$ threshold at a higher rate. We suggest that this is further evidence that SL-GRBs are a discrete population of bursts.

We have shown that the methods presented here are strongly dependent on the event rate density of the sources and a good description of the scaling function $S(L)$ is not essential. Additionally, in the redshift regime where the method is dependent on only the closest events, high- z biases do not effect the analysis. Used in the peak flux regime, the method depends on only the brightest of bursts which are less likely to be missed because of detection thresholds. We suggest that an observation-time analysis is a useful complement to other methods that use the whole distribution and can be a good indicator of selection bias.

The $\log P - \log T$ method, in comparison with a $\log Z - \log T$ technique can not be used to discriminate between populations occurring at different rates. A close burst could arise from the low luminosity tail of the LF and equivalently a distant burst would be intrinsically bright. Therefore a $\log Z - \log T$ relation which has only a spacial dependence is a stronger indicator. As an intrinsic luminosity is determined from both the redshift and peak flux, a $\log L - \log T$ relation, which includes a measure of both the energy and spacial distribution could prove useful. Such a relation may be useful to untangle populations such as SGRBs and SGRB-EEs which have similar redshift distributions.

We analysed the burst GRB 060505 using the $\log Z - \log T$ relation to determine if it could be of the SL-GRB category. Including this burst with the other two *Swift* SL-

GRBs, GRB 060218 and GRB 100316D, we found that all three bursts were constrained at rate $\rho_{0,SL} = 147\text{Gpc}^{-3}\text{yr}^{-1}$ estimated independently by a V_{MAX} analysis. Therefore, in addition to its low-luminosity and relative close proximity a $\log Z - \log T$ analysis supports the hypothesis that this burst is a SL-GRB. In contrast to other SL-GRBs, despite intense photometric and spectroscopic searches, this burst showed no evidence of an associated supernova. To tests its compatibility with the SGRB population, we performed a further $\log Z - \log T$ analysis and found a greater than 99% probability that a SGRB would not have occurred as close as this burst.

If the progenitor of GRB 060505 was not a compact object merger, upper limits on the ejected ^{56}Ni mass of $M(^{56}\text{Ni}) \sim 10^{-3}M_{\odot}$ (Tominaga et al. 2007) support the possibility that this burst may have been accompanied by a low energy SN undergoing significant fallback (Woosley & Weaver 1995; Fryer et al. 2006).

An additional analysis of the burst GRB 080905A shows how the $\log Z - \log T$ relation can select out bursts with anomalous properties from a given sample. Using the method in a bootstrapping type scheme may be a useful consistency test for both the completeness of sample selections and some of the spectral energy relations related to the observed quantities of GRBs (e.g. Amati et al. 2002; Yonetoku et al. 2004; Ghirlanda et al. 2005).

ACKNOWLEDGMENTS

E. J. Howell acknowledges support from a UWA Research Fellowship. D.M. Coward is supported by an Australian Research Council Future Fellowship. The authors thank the referee for a thorough reading of the manuscript and for providing a number of insightful suggestions.

APPENDIX A: THE DIFFERENTIAL PEAK FLUX DISTRIBUTION DATA OF BATSE AND SWIFT LGRBS

P1 ph sec ⁻¹ cm ⁻²	P2 ph sec ⁻¹ cm ⁻²	\dot{N} yr ⁻¹	$\Delta\dot{N}/\Delta P$ yr ⁻¹ ph sec cm ²
0.4	0.51	25	222
0.51	0.66	22	145
0.66	0.84	20	113
0.84	1.1	17	88.2
1.1	1.4	15	61
1.4	1.8	13	38.4
1.8	2.3	11	24.6
2.3	2.9	8.8	15
2.9	3.7	7.2	8.78
3.7	6.1	11	4.64
6.1	7.8	3.8	2.44
7.8	10	3	1.5
10	13	2.4	1.06
13	16	1.9	0.415
16	21	1.5	0.324
21	44	2.7	0.129

Table A1. The data used in fitting the differential peak flux distribution of the BATSE long GRB sample

P1 ph sec ⁻¹ cm ⁻²	P2 ph sec ⁻¹ cm ⁻²	\dot{N} yr ⁻¹	$\Delta\dot{N}/\Delta P$ yr ⁻¹ ph sec cm ²
0.4	0.56	9.7	59
0.56	0.8	7.8	33.4
0.8	1.1	11	34.6
1.1	1.6	8.9	19.1
1.6	2.2	11	16.3
2.2	3.2	6.7	7.2
3.2	4.5	3.8	2.87
4.5	6.3	3.6	1.95
6.3	8.9	3.8	1.44
8.9	13	1.8	0.49
13	18	0.97	0.187
18	25	1.7	0.227
25	50	0.97	0.0388

Table A2. The data used in fitting the differential peak flux distribution of the *Swift* long GRB sample

APPENDIX B: PEH REDSHIFT DATA

Table B1. The Swift redshift-observation-time data $Z(T)$ used in the analysis. The data is taken from December 19 2004 and re-ordered as a time-series using the *FromMIN* method. The PEH data is shown as bold.

GRB	T_{obs}	redshift	GRB	T_{obs}	redshift	GRB	T_{obs}	redshift
050904	8	6.29	071117	811	1.331	091018	1512	0.971
050908	12	3.344	071122	816	1.14	091020	1514	1.71
050922C	26	2.198	080129	888	4.349	091024	1518	1.092
051016B	50	0.9364	080207	896	2.2	091029	1523	2.752
051109A	73	2.346	080210	899	2.641	091109A	1533	3.076
051111	75	1.55	080310	929	2.42	091127	1551	0.49
060115	144	3.53	080319B	938	0.937	091208B	1562	1.063
060124	153	2.296	080319C	938	1.95	100219A	1638	4.6667
060202	161	0.783	080330	949	1.51	100302A	1651	4.813
060206	165	4.048	080411	960	1.03	100316B	1665	1.18
060210	169	3.91	080413A	962	2.433	100418A	1697	0.6235
060223A	182	4.41	080413B	962	1.1	100425A	1704	1.755
060418	237	1.489	080430	979	0.767	100513A	1722	4.772
060502A	251	1.51	080520	999	1.545	100621A	1760	0.542
060510B	259	4.9	080603B	1012	2.69	100724A	1793	1.288
060512	261	2.1	080604	1013	1.416	100728B	1797	2.106
060522	271	5.11	080605	1014	1.6398	100814A	1813	1.44
060526	275	3.221	080607	1016	3.036	100901A	1830	1.408
060604	283	2.68	080707	1046	1.23	100906A	1835	1.727
060605	284	3.78	080710	1049	0.845	101219B	1938	0.55
060607A	286	3.082	080721	1060	2.591	110106B	1960	0.618
060707	316	3.425	080804	1073	2.2045	110128A	1982	2.339
060708	317	1.92	080805	1074	1.505	110205A	1989	2.22
060714	323	2.711	080810	1079	3.35	110213A	1997	1.46
060729	338	0.54	080905B	1104	2.374	110213B	1997	1.083
060814	353	0.84	080906	1105	2.1	110422A	2066	1.77
060904B	373	0.703	080913	1112	6.695	110503A	2077	1.613
060906	375	3.686	080916A	1115	0.689	110715A	2149	0.82
060908	377	1.8836	080928	1127	1.692	110731A	2165	2.83
060912A	381	0.937	081007	1136	0.5295	110801A	2165	1.858
060926	395	3.2	081008	1137	1.9685	110808A	2172	1.348
060927	396	5.47	081028A	1157	3.038	110818A	2182	3.36
061007	406	1.261	081029	1158	3.8479	111008A	2232	4.9898
061021	420	0.3463	081118	1177	2.58	111107A	2261	2.893
061110A	439	0.758	081121	1180	2.512	111209A	2293	0.677
061110B	439	3.44	081203A	1192	2.05	111228A	2312	0.714
061121	450	1.314	081222	1211	2.77	111229A	2313	1.3805
061126	455	1.1588	081228	1217	3.4	120119A	2338	1.728
061222A	481	2.088	081230	1219	2	050126	2381	1.29
061222B	481	3.355	090102	1226	1.547	050223	2408	0.5915
070110	504	2.352	090205	1259	4.6497	050315	2430	1.949
070208	532	1.165	090313	1297	3.375	050318	2433	1.44
070306	560	1.4959	090417B	1331	0.345	050319	2434	3.24
070318	572	0.836	090418A	1332	1.608	050401	2446	2.9
070411	595	2.954	090423	1337	8.26	050505	2480	4.27
070419A	603	0.97	090424	1338	0.544	050525A	2500	0.606
070506	620	2.31	090426	1340	2.609	050603	2508	2.821
070521	635	1.35	090429B	1343	9.2	050730	2565	3.967
070529	643	2.4996	090516A	1360	4.109	050801	2566	1.56
070611	655	2.04	090519	1363	3.85	050814	2579	5.3
070612A	656	0.617	090529	1373	2.625	050820A	2585	2.612
070721B	695	3.626	090530	1374	1.3	050826	2591	0.297
070802	706	2.45	090618	1392	0.54			
070810A	714	2.17	090715B	1419	3			
071003	767	1.6043	090726	1430	2.71			
071010A	774	0.98	090809	1443	2.737			
071010B	774	0.947	090812	1446	2.452			
071020	784	2.145	090814A	1448	0.696			
071031	795	2.692	090926B	1490	1.24			
071112C	806	0.823	090927	1491	1.37			

REFERENCES

- Amati L., et al., 2002, *A&A*, 390, 81
- Band D., 2003, *ApJ*, 588, 945
- Bloom J. S., Butler N. R., Perley D. A., 2008, in M. Galassi, D. Palmer, & E. Fenimore ed., *American Institute of Physics Conference Series Vol. 1000*, . p. 11
- Borgonovo L., Björnsson C.-I., 2006, *ApJ*, 652, 1423
- Bromberg O., Nakar E., Piran T., Sari R., 2012, *ApJ*, 749, 110
- Bucciantini N., Metzger B. D., Thompson T. A., Quataert E., 2012, *MNRAS*, 419, 1537
- Butler N. R., Bloom J. S., Poznanski D., 2010, *ApJ*, 711, 495
- Campana S., et al., 2006, *A&A*, 454, 113
- Campisi M. A., Li L.-X., Jakobsson P., 2010, *MNRAS*, 407, 1972
- Carroll S. M., Press W. H., Turner E. L., 1992, *ARAA*, 30, 499
- Chapman R., Priddey R. S., Tanvir N. R., 2009, *MNRAS*, 395, 1515
- Cobb B. E., et al., 2006, *ApJ*, 645, L113
- Coward D., 2007, *New. A. Rev.*, 51, 539
- Coward D., Howell E., Piran T., Stratta G., Branchesi M., Bromberg O., Gendre B., Burman R., Guetta D., 2012, submitted to *MNRAS*; preprint:astro-ph/1202.2179
- Coward D. M., 2005, *MNRAS*, 360, L77
- Coward D. M., Burman R. R., 2005, *MNRAS*, 361, 362
- Coward D. M., Guetta D., Burman R. R., Imerito A., 2008, *MNRAS*, 386, 111
- Coward D. M., Lilley M., Howell E. J., Burman R. R., Blair D. G., 2005, *MNRAS*, 364, 807
- Cucchiara A., et al., 2011, *ApJ*, 736, 7
- Daigne F., Mochkovitch R., 2007, *A&A*, 465, 1
- Elliott J., Greiner J., Khochfar S., Schady P., Johnson J. L., Rau A., 2012, *A&A*, 539, A113
- Fasano G., Franceschini A., 1987, *MNRAS*, 225, 155
- Feng L., Fox D. B., 2010, *MNRAS*, 404, 1018
- Fruchter A. S., et al., 2006, *Nature*, 441, 463
- Fryer C. L., Young P. A., Hungerford A. L., 2006, *ApJ*, 650, 1028
- Fynbo J., et al., 2006, *Nature*, 444, 1047
- Gehrels N., 1986, *ApJ*, 303, 336
- Ghirlanda G., Ghisellini G., Firmani C., Celotti A., Bosnjak Z., 2005, *MNRAS*, 360, L45
- Greiner J., et al., 2008, submitted to *ApJ*, preprint:astro-ph/0810.2314
- Gruber D., for the Fermi/GBM collaboration 2012 Rest-frame properties of gamma-ray bursts observed by the Fermi Gamma-Ray Burst Monitor
- Grupe D., Burrows D. N., Patel S. K., Kouveliotou C., Zhang B., Mészáros P., Wijers R. A. M., Gehrels N., 2006, *ApJ*, 653, 462
- Guetta D., Della Valle M., 2007, *ApJL*, 657, L73
- Guetta D., Piran T., 2007, *J. Cosmol. Astropart. Phys.*, 2007, 003
- Guetta D., Piran T., Waxman E., 2005, *ApJ*, 619, 412
- Guetta D., Stella L., 2009, *A&A*, 498, 329
- Hjorth J., 2003, *Nature*, 423, 847
- Hopkins A. M., Beacom J. F., 2006, *ApJ*, 651, 142
- Horváth I., 1998, *ApJ*, 508, 757
- Horváth I., 2009, *Ap&SS*, 323, 83
- Horváth I., Bagoly Z., Balázs L. G., de Ugarte Postigo A., Veres P., Mészáros A., 2010a, *ApJ*, 713, 552
- Horváth I., Bagoly Z., Balázs L. G., de Ugarte Postigo A., Veres P., Mészáros A., 2010b, *ApJ*, 713, 552
- Howell E., Coward D., Burman R., Blair D., 2007a, *MNRAS*, 377, 719
- Howell E., Coward D., Burman R., Blair D., 2007b, *ApJ*, 666, L65
- Howell E., Coward D., Burman R., Blair D., 2010, in *American Institute of Physics Conference Series Vol. 1246*, . p. 203
- Howell E., Regimbau T., Corsi A., Coward D., Burman R., 2011, *MNRAS*, 410, 2123
- Imerito A., et al., 2008, *MNRAS*, 391, 405
- Kann D. A., et al., 2011, *ApJ*, 734, 96
- Kommers J. M., Lewin W. H. G., Kouveliotou C., van Paradijs J., Pendleton G. N., Meegan C. A., Fishman G. J., 2000, *ApJ*, 533, 696
- Kouveliotou C., et al., 1993, *ApJ*, 413, L101+
- Li L., 2008, *MNRAS*, 388, 1487
- Liang E., et al., 2007, *ApJ*, 662, 1111
- Malesani D., et al., 2007, *A&A*, 473, 77
- McBreen S., et al., 2008, *ApJL*, 677, L85
- Mészáros A., 2006, *Reports on Progress in Physics*, 69, 2259
- Mészáros A., Bagoly Z., Balázs L. G., Horváth I., 2006, *A&A*, 455, 785
- Meszáros A., Meszaros P., 1996, *ApJ*, 466, 29
- Mészáros A., Rípa J., Ryde F., 2011, *A&A*, 529, A55
- Meszáros P., Meszaros A., 1995, *ApJ*, 449, 9
- Metzger B. D., Quataert E., Thompson T. A., 2008, *MNRAS*, 385, 1455
- Modjaz M., et al., 2008, *ApJ*, 135, 1136
- Mukherjee S., Feigelson E. D., Jogesh Babu G., Murtagh F., Fraley C., Raftery A., 1998, *ApJ*, 508, 314
- Murase K., et al., 2006, *ApJ*, 651, L5
- Nakar E., 2007, *Phys.Rept*, 442, 166
- Norris J. P., Bonnell J. T., 2006, *ApJ*, 643, 266
- Norris J. P., Gehrels N., Scargle J. D., 2010, *ApJ*, 717, 411
- Norris J. P., Gehrels N., Scargle J. D., 2011, *ApJ*, 735, 23
- Norris J. P., Marani G. F., Bonnell J. T., 2000, *ApJ*, 534, 248
- Ofek E. O., et al., 2007, *ApJ*, 662, 1129
- Paciesas W. S., et al., 1999, *ApJS*, 122, 465
- Page K. L., et al., 2006, *ApJL*, 637, L13
- Peacock J. A., 1983, *MNRAS*, 202, 615
- Perley D. A., et al., 2008, submitted to *ApJ*, preprint:astro-ph/0811.1044
- Pian E., et al., 2006, *Nature*, 442, 1011
- Porciani C., Madau P., 2000, *ApJ*, 548, 522
- Reichart D. E., Meszaros P., 1997, *ApJ*, 483, 597
- Rowlinson A., et al., 2010, *MNRAS*, 408, 383
- Sakamoto T., et al., 2011, *ApJS*, 195, 2
- Sakamoto T., Hullinger D., Sato G., Yamazaki R., Barbier L., Barthelmy S. D., Cummings J. R., Fenimore E. E., Gehrels N., Krimm H. A., Lamb D. Q., Markwardt C. B., Osborne J. P., Palmer D. M., Parsons A. M., Stamatikos M., Tueller J., 2008, *ApJ*, 679, 570
- Salvaterra R., Chincarini G., 2007, *ApJL*, 656, L49
- Salvaterra R., Guidorzi C., Campana S., Chincarini G., Tagliaferri G., 2009, *MNRAS*, 396, 299
- Soderberg A. M., et al., 2006, *Nature*, 422, 1014
- Stanek K., 2003, *ApJ*, 591, L17

- Starling R. L. C., et al., 2011, *MNRAS*, 411, 2792
- Thoene C. C., Fynbo J. P. U., 2007, ArXiv e-prints
- Thöne C. C., et al., 2008, *ApJ*, 676, 1151
- Tominaga N., Maeda K., Umeda H., Nomoto K., Tanaka M., Iwamoto N., Suzuki T., Mazzali P. A., 2007, *ApJL*, 657, L77
- Řípa J., Mészáros A., Wigger C., Huja D., Hudec R., Hajdas W., 2009, *A&A*, 498, 399
- Vavrek R., Balázs L. G., Mészáros A., Horváth I., Bagoly Z., 2008, *MNRAS*, 391, 1741
- Veres P., Bagoly Z., Horváth I., Mészáros A., Balázs L. G., 2010, *ApJ*, 725, 1955
- Vink J. S., de Koter A., 2005, *A&A*, 442, 587
- Virgili F. J., Liang E., Zhang B., 2009, *MNRAS*, 392, 91
- Virgili F. J., Liang E.-W., Zhang B., 2008, *MNRAS*, 392, 91
- Wall J. V., Jenkins C. R., Ellis R., Huchra J., Kahn S., Rieke G., Stetson P. B., 2003, *Practical Statistics for Astronomers*
- Wanderman D., Piran T., 2010, *MNRAS*, 406, 1944
- Wosley S., Janka T., 2005, *Nature Physics*, 1, 147
- Wosley S. E., Bloom J. S., 2006, *Annu. Rev. Astro. Astrophys.*, 44, 507
- Wosley S. E., Heger A., 2006, *ApJ*, 637, 914
- Wosley S. E., Weaver T. A., 1995, *ApJS*, 101, 181
- Xu D., et al., 2009, *ApJ*, 696, 971
- Yonetoku D., Murakami T., Nakamura T., Yamazaki R., Inoue A. K., Ioka K., 2004, *ApJ*, 609, 935
- Zhang B., 2006, *Nature*, 444, 1010
- Zhang B., 2007, *Chin. J. Astron. Astrophys.*, 7, 1
- Zhang B., 2011, *Comptes Rendus Physique*, 12, 206
- Zhang B., et al., 2007, *ApJ*, 655, L25